JOURNAL OF MATERIALS SCIENCE 30 (1995) 4299–4308

Characterization of bismuth lead oxide by vibrational spectroscopy

N. M. SAMMES, G. TOMPSETT, A. M. CARTNER*
*Centre for Technology, and *Department of Chemistry, The University of Waikato, Private Bag 3105, Hamilton, New Zealand*

Bismuth lead oxide is a promising fast-ion conductor, with an oxygen ion conductivity in excess of 1 S cm^{-1} at 590 °C. The characterization of the system $(Bi_2O_3)_{1-x}$ $(PbO)_x$ has previously been investigated using powder X-ray diffractometry; however, a detailed study using vibrational spectroscopy has not been carried out. This work examines the phases present between $x=0$ and 1 using both infrared and Raman spectroscopy. Detailed spectra of the phases are included, as well as an analysis of those phases. In general, the phases are reasonably consistent with previously published data; however, certain aspects differ. γ-$Bi_{12}PbO_{19}$, for example, was found to be a solid solution stable over a wide range of PbO, rather than a single phase as previously published. A summary of the room-temperature phases, after having been quenched from specific temperatures, is included in the form of a proposed phase diagram.

1. Introduction

Polymorphs of Bi_2O_3 have been the subject of a number of investigations [1–3]. Pure Bi_2O_3 shows a monoclinic α-phase, stable at temperatures below 730 °C and a face centred cubic (fcc) structure (δ-phase) stable above 730 °C to its melting point of 824 °C. Cooling the sample from the δ-range produces a large thermal hysteresis which may allow for the formation of one of two metastable phases; the body centred cubic (bcc) γ-phase or the tetragonal β-phase [4]. These phases usually transform back to the α-phase in the temperature range 650–500 °C.

Low-temperature stabilization of the high-temperature δ-phase has been examined in great detail, due to its relatively high ionic conductivity [5–7]. The addition of PbO to Bi_2O_3 induces a range of phases, stable at room temperature, depending on the dopant concentration. Early work by Levin and Roth [8] suggested that a bcc structure could be stabilized at low dopant concentrations, while the later work of Boivin and Tridot [9] and Biefeld and White [10] suggested a range of metastable phases could be formed, depending on the percentage of lead present. Of particular interest was the formation of the bcc β-phase, which was stable above 590 °C, over a wide range of composition, and was later found to have an oxygen ionic conductivity greater than 1 S cm^{-1} [11, 12]. At lower temperatures, the β-phase transforms to either a tetragonal β_2 or a monoclinic solid solution (β_1). Honnart *et al.* [12] also showed that the high-temperature β-phase could not be quenched in.

At lower concentrations of PbO, other phases were noted, including a number of compounds with limited composition ranges. The most interesting compound to be formed was that of $Bi_8Pb_5O_{17}$ (formed at a dopant level of 55.5 mol % PbO), which had a very well-defined transformation temperature and very high ionic conductivity [12].

Several Bi_2O_3–PbO phase equilibrium diagrams have been attempted [9, 13, 14], most recently by Biefeld and White [10]. The results are, in part, contradictory and at times misleading. The results from these studies were obtained from room-temperature and high-temperature powder X-ray diffraction and it was not clear whether the phases were obtained by quenching the sample or by equilibrium cooling. Little previous work is available in the literature on the infrared or Raman spectra for the Bi_2O_3-PbO system, presumably due to the metastability and complexity of the phases present. Only α-Bi_2O_3 has been studied in detail [15–17], and was found to be monoclinic belonging to the space group $P2_{1/c}$ (C_{2h}^5), with 4 Bi_2O_3 per unit cell. The factor group analysis predicted a total of 27 active infrared modes and 30 Raman modes, with no coincidence. The Raman spectrum of α-Bi_2O_3 at 298 K was found to exhibit 15 bands, whereas the infrared spectrum exhibited 16 bands [15].

Betsch and White [15] also studied Raman and infrared spectra of the sillenite structure of the bismuth oxide (γ phase) including the compound $Bi_{12}PbO_{19}$. The sillenite structure was found to have the bcc space group I23 (T^3) with two formula units in the unit cell. Factor group analysis predicted a total of 23 infrared active modes and 40 Raman active modes. Seven main bands in the Raman spectra at 50, 78, 132, 145, 251, 317 and 531 cm^{-1} were observed for the $Bi_{12}PbO_{19}$ structure at room temperature and 11 bands at 47, 82, 106, 110, 170, 222, 300, 465, 520, 575 and 630 cm^{-1} in the infrared spectrum.

0022–2461

Hardcastle and Wachs [16] reported the Raman spectra for the phases of α, β, and δ for the bismuth oxide system. Bands for β-Bi_2O_3 were reported at approximately 127, 147, 294, 307 and 450 cm^{-1}, while for δ-Bi_2O_3 at approximately 563–570 cm^{-1}, using bismuth oxide doped with molybdenum oxide as a comparison.

Bond strengths and (co-ordination) of bismuth, and hence Raman spectral positions, have been empirically calculated for bismuth oxide phases [16]. However, there are no further reported infrared or Raman spectra of bismuth (lead) oxide in the literature, although there are a number of authors who have reported work on other doped bismuth oxide systems [17–19]. It was, therefore, the object of this study to obtain further understanding of the room-temperature phases present in the Bi_2O_3–PbO system by vibrational spectroscopy.

2. Experimental procedure

Bi_2O_3 (Rectapur 99%) and PbO (Analar 99%) were mixed in the correct stoichiometric proportions to form $(Bi_2O_3)_{1-x}(PbO)_x$ (from $x = 0$–1.0). The samples were repeatedly ground in a mortar and pestle to remove any agglomerates present. The samples were then die-pressed into discs (15 mm diameter) and sintered at varying temperatures up to 750 °C on crystalline magnesia for 2 h. Powder X-ray diffraction, using a Philips powder X-ray diffractometer (CuK_α radiation), was undertaken on the discs and the firing and grinding sequences were repeated until no further changes in phase were observed. The samples were removed from the furnace by air quenching, although other cooling regimes were examined. Raman spectroscopy was performed on the samples using a Spex 1403 0.84 m double beam pass spectrometer equipped with a Spectra Physics model 164 argon-ion laser, a Spectra Physics HeNe laser model 207B, and a water-cooled Hammamatsu R943-02 photomultiplier tube. Unless otherwise noted, spectra were recorded at 5 cm^{-1} resolution using a 488 nm laser line at a laser output power of 100–200 mW, with incident power at approximately 50 mW, or a 632 nm laser line for the HeNe laser at 25 mW. The scanning rate used to collect the spectra was kept at 0.5 $cm^{-1}\,s^{-1}$. The spectrometer was interfaced to a DM1B computer to provide for spectrometer control as well as multiple scans and data manipulation. The fired samples were ground into powders using a mortar and pestle, and either analysed in glass capillary tubes, or scanned as pressed discs, oriented at approximately 45° to the incident beam.

Infrared spectroscopy was performed on a Digilab FTS-40 Fourier transform–infrared spectrometer, employing an evacuated far-IR bench. The spectra were examined in the range 30–700 cm^{-1}. The fired samples were again ground into powders and examined as vaseline mulls between thin polyethylene plates.

Low-temperature Raman spectroscopy was undertaken using a double beam pass Jobin Yvon U-1000 Raman spectrometer, equipped with a microscope stage for analysing small samples with 180° incident geometry. A Spectra-Physics argon-ion laser was employed to excite laser Raman spectra using the 514 nm laser line and 25–50 mW power, along with 500 μm slits. A LINKAM TMS-91 temperature stage attachment to the microscope coupled with a CS196 cooling system and thermal monitor, was used to cool samples to − 195 °C, using liquid nitrogen, and to heat them to 600 °C. Spectra were obtained using an uncoated Olympus × 20 objective lens and at a scanning rate of 0.5 $cm^{-1}\,s^{-1}$ over a range of 25–1000 cm^{-1}.

3. Results and discussion

Fig. 1 shows the Raman spectral profiles for the $(Bi_2O_3)_{1-x}(PbO)_x$ samples from $x = 0$–0.25, after having been sintered and quenched from a number of different composition-determined temperatures. Table I lists the Raman band positions, as well as the quenching temperature, for all the samples investigated (from $x = 0$–1). The band positions are identified by comparison with those in the literature for α-Bi_2O_3, β-Bi_2O_3, γ-Bi_2O_3, δ-Bi_2O_3 and γ-PbO.

Fourteen bands were observed for α-Bi_2O_3 standard laboratory reagent ($x = 0$), at room temperature, with two broad, strong bands at 315 and 448 cm^{-1}. The profile is one of broad, high wavenumber bands and narrow, low wavenumber (< 250 cm^{-1}) bands.

For the PbO ($0 < x \leqslant 0.25$)-doped Bi_2O_3 systems, samples were investigated by quenching from within the δ-Bi_2O_3 region and from within the δ-Bi_2O_3 + β region (as described by the phase equilibrium diagram given by Biefeld and White [10]). The Raman spectra show a gradual shift from a profile that resembles α-Bi_2O_3 with extra bands at 69, 252, 537, 651 and 645 cm^{-1}. At $x = 0.1$ there is a total profile change with predominant bands at 50, 80, 124, 318 and 533 cm^{-1}. This profile is comparable to that observed by Betsch and White [15] for the sillenite structure, $Bi_{12}PbO_{19}$. There is no evidence of α-Bi_2O_3 present because the strong band at 448 cm^{-1} does not occur. Overall, there are 14 bands observed for this stoichiometry, with the same profile being observed for $x = 0.12$, 0.13, 0.143, 0.16, 0.18, 0.20 and 0.25 with a small amount of α-Bi_2O_3 being detected for $x = 0.18$, 0.143 and 0.16, indicated by weak bands at 108 and 433 cm^{-1}.

Samples of composition $x = 0.18$ show only the band profile described by the γ-$Bi_{12}PbO_{19}$ also shown in the $x = 0.10$ and 0.12 samples with a more intense band at 149 cm^{-1}. As x is increased to greater than 0.18, the profile is that of γ-$Bi_{12}PbO_{19}$ with an increasing intensity of the band at 146 cm^{-1} and a shoulder band at ~ 500 cm^{-1}, with increasing x. These additional bands have been assigned the β_2-$Bi_8Pb_5O_{17}$ composition and were quenched from the δ-Bi_2O_3 + β region. These phases were described by Boivin and Tridot [9], who used powder X-ray diffraction methods, as forming α-Bi_2O_3 and $Bi_{12}PbO_{19}$, at $0 < x < 0.143$, after being quenched from the δ-Bi_2O_3 region, pure $Bi_{12}PbO_{19}$ at $x = 0.143$, and $Bi_{12}PbO_{19}$ plus β_2 at $0.143 < x < 0.149$, with the β_1 phase being observed between $x = 0.42$ and 0.46.

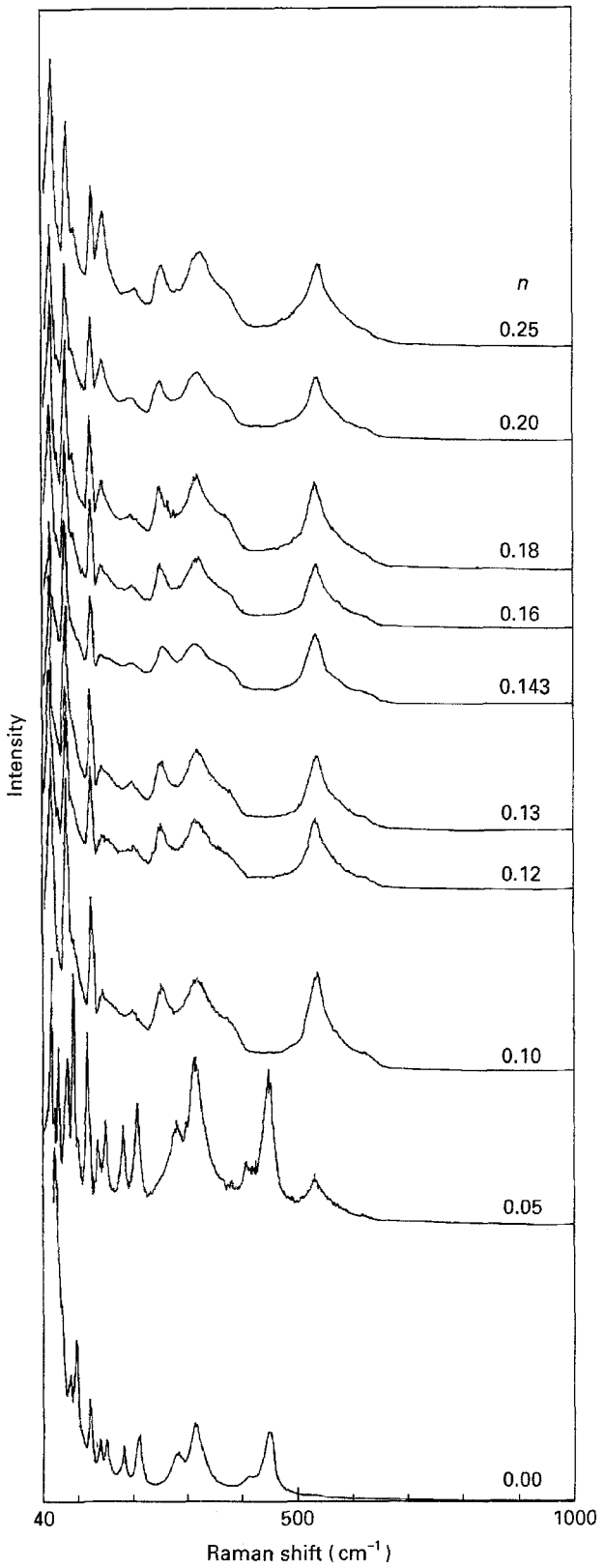

Figure 1 Raman spectra of $(Bi_2O_3)_{1-x}(PbO)_x$, where $x = 0.00$–0.25.

At the γ-$Bi_{12}PbO_{19}$ stoichiometry ($x = 0.143$) several quenching temperatures were used to determine the presence of the eutectoid. The temperatures were 650 °C (below the eutectoid line), 700 °C (within the eutectoid range) and 750 °C (above the eutectoid). The Raman spectra are shown in Fig. 2 and at 650 and 700 °C, the presence of α-Bi_2O_3 is clearly distinguishable with a component of γ-$Bi_{12}PbO_{19}$ also present. Quenching from 750 °C, however, produces a Raman spectra indicative of γ-$Bi_{12}PbO_{19}$ with trace amounts of α-Bi_2O_3, indicated by a weak band at 448 cm^{-1}.

Because the γ-$Bi_{12}PbO_{19}$ spectral profile is observed for a range of compositions ($x = 0.05$–0.25 and 0.3, described later), it indicates that a stable solid solution must be present as opposed to a single (sillenite) compound as implied by Betsch and White [15]. Both the $x = 0.10$ and 0.12 samples, in this work, show no evidence of α-Bi_2O_3, indicating that the γ-$Bi_{12}PbO_{19}$ solid solution can be stabilized over a wider range of PbO, on the low PbO side of the eutectoid, rather than just at 0.12 given in the phase diagram described by Biefeld and White [10]. The γ-$Bi_{12}PbO_{19}$ has been renamed δ', by us, because the evidence suggests that rather than a single sillenite phase, a solid solution can be formed over a range of compositions, after quenching from the high-temperature δ-phase.

Raman spectra for $x = 0.3$–0.8 are shown in Fig. 3, and further described in Table I. The Raman spectrum at $x = 0.3$ reveals two major components; γ-$Bi_{12}PbO_{19}$ and β_2-$Bi_8Pb_5O_{17}$. This appears to be inconsistent with the phase equilibrium diagram because only the β_2-phase is expected. At this stage the reason for this is not fully understood; however, it can be postulated that certain changes to the phase equilibrium diagram are necessary to take into account all the observations noted in this work.

At $x = 0.35$, the Raman profile shows a distinct difference, indicating the formation of a new phase or solid solution. Between 0.35 and 0.45, there is a shift in the band maximum, in particular the band at 136 cm^{-1}, which is maximum for $x = 0.4$. At this composition, the stoichiometric composition $3Bi_2O_3 \cdot 2PbO$ ($Bi_6Pb_2O_{11}$) has been assigned to this system by both Boivin and Tridot [9] and Biefeld and White [10], forming the β_1 phase on quenching. This phase appears to be only stable over a very narrow composition range. Moreover, the phase composition is best defined by the stoichiometric point, with no evidence of the β_2 phase after quenching, as expected from the phase equilibrium diagram. Therefore, it seems likely that the phase equilibrium diagram should contain a very narrow β-region at this ($x = 0.4$) composition.

At $x = 0.5$, there is again a unique Raman profile, consistent for compositions $x = 0.5$–0.7, including 0.555. This indicates that it is due to the β_2-phase of Bi_2O_3–PbO and is a major phase stabilized over its composition range. The most distinctive feature is an intense band at 145 cm^{-1}.

At higher compositions, the presence of orthorhombic PbO is evident from the intense spectral features at 142 and 290 cm^{-1}, which is in agreement with the phase equilibrium diagram.

Low-temperature Raman spectra for $x = 0.143$, 0.4, 0.555 and 0.74 are given in Fig. 4a–d. The Raman spectra for $x = 0.143$ at room temperature (21 °C) and − 195 °C is given in Fig. 4a. At room temperature, 16 bands are visible at 50, 78, 123, 142, 156, 201, 251, 291, 314, 364, 450, 528, 565, 588, 615 and 826 cm^{-1}, whereas at − 195 °C, 21 bands were observed, including six shoulders to other bands, at positions 42 (sh), 53 (vs),

TABLE I Raman band positions of Bi_2O_3 and Bi_2O_3–PbO at room temperature

PbO:Bi_2O_3 (n)	Preparation description	Compound	Phase	Raman band positions (relative intensity) (cm^{-1})	Reference
0	Lab reagent	α-Bi_2O_3	Major	54 (s), 67(w), 82(w), 94(m), 119(s), 139(m), 152(m), 184(m), 212(m), 281(m,b), 315(s,b), 413(w,b), 448(s,b), 529 (w)	Present work
0	Lab reagent	α-Bi_2O_3	Major	53, 59, 67, 83, 93, 102, 118, 139, 151, 184, 210, 282, 314, 410, 446	[15]
0		β-Bi_2O_3		127(w, sh), 147(vs), 294(s), 450(vw)	[17]
0		δ-Bi_2O_3		563(m)	[17]
0.143	700 °C for 24 h	$Bi_{12}PbO_{19}$		50(s), 78(s), 132(m), 145(w), 251(m), 317(m), 531(m)	[15]
0.05	750 °C for 2 h and quenched	α-Bi_2O_3	Major	55(s), 62(w), 69(s), 85(m), 96(s), 105(w), 121(s), 141(m), 153(m), 186(m), 212(m), 282(w), 317(w), 417(w), 449(m)	Present work
					Present work
		$Bi_{12}PbO_{19}$	Minor	69(s), 252(sh), 532(w), 651(sh), 645(w)	Present work
0.1	750	$Bi_{12}PbO_{19}$	Major	50(s), 64(w), 80(s), 92(sh), 124(s), 145(w), 159(w), 199(w), 251(w), 318(m,b), 366(sh), 533(m), 571(sh), 624(w)	Present work
0.12	750	$Bi_{12}PbO_{19}$	Major	53(s), 66(w), 81(s), 91(sh), 126(s), 149(w), 200(w), 252(w), 317 (m), 363(sh), 534(m), 565(sh), 620(w)	Present work
0.13	750	$Bi_{12}PbO_{19}$	Major	51(s), 63(w), 79(s), 92(w), 123(s), 143(w), 157(sh), 200(w), 251(w), 319(m), 387(sh), 535(m), 572(sh), 618(w)	Present work
		α-Bi_2O_3	Minor	108(w), 433(vw)	Present work
0.143	650	α-Bi_2O_3	Major	54(s), 60(w), 68(s), 84(s), 95(s), 103(w), 120(s), 140(m), 153(m), 185(m), 212(m), 283(w), 314(s), 411(w), 449(m)	Present work
		$Bi_{12}PbO_{19}$	Minor	253(sh), 452(m), 567(sh), 615(w)	Present work
0.143	700	α-Bi_2O_3	Major	53(s), 68(m), 83(m), 94(s), 103(w), 119(s), 140(m), 152(m), 212(m), 281(w), 351(s), 411(w), 449(s),	Present work
		$Bi_{12}PbO_{19}$	Minor	248(sh), 532(w), 576 (sh), 621(w)	Present work
0.143	750	$Bi_{12}PbO_{19}$	Major	52(s), 79(s), 92(sh), 122(m), 143(w), 158(sh), 199(w), 252(w), 314(m), 363(sh), 530(s), 569(sh), 618(w)	Present work
0.16	750	$Bi_{12}PbO_{19}$	Major	51(s), 63(w), 79(s), 90(sh), 124(m), 143(w), 161(sh), 199(w), 251(w), 316(m), 374(sh), 533(m), 572(sh), 618(w)	Present work
		α-Bi_2O_3	Minor	109(vw), 446(vw)	Present work
0.18	750	$Bi_{12}PbO_{19}$	Major	54(s), 67(w), 82(s), 95(sh), 127(s), 149(w), 202 (w,b), 255(w), 319(m), 371(sh), 536(m), 569(sh), 616(w)	Present work
		β_2-$Bi_8Pb_5O_{17}$	Minor	54(s), 149(w), 500(sh)	Present work
0.20	750	$Bi_{12}PbO_{19}$	Major	50(s), 61(w), 78(s), 92(sh), 122(m), 142(w), 154(sh), 200(w), 249(w). 318(m,b), 360(sh), 533(m), 569(sh), 621(w)	Present work
		β_2-$Bi_8Pb_5O_{17}$	Minor	142(w)	Present work
		α-Bi_2O_3	Major	109(w), 446(v,w)	Present work
0.25	700	$Bi_{12}PbO_{19}$	Major	51(s), 62 (w), 79(s), 91(w), 123(m), 200(w), 252(w), 319(m), 367(sh), 534(m), 569(sh), 622(w)	Present work
		β_2-$Bi_8Pb_5O_{17}$	Minor	146(m), 494(sh)	Present work
0.30	700	$Bi_{12}PbO_{19}$	Major	52(s), 65(sh), 80(s), 92(sh), 125(m), 201(w), 252(w), 318(m), 364(sh), 564(m), 596(sh), 632(sh)	Present work
		β_2-$Bi_8Pb_5O_{17}$	Major	143(m), 491(m)	Present work
0.35	690	β_1-$Bi_6Pb_2O_{11}$	Major	74(w), 92(w), 133(w), 161(sh), 295(w,b), 488(m), 588(w,b)	Present work
0.40	670	β_1-$Bi_6Pb_2O_{11}$	Major	49(w), 84(m), 96(s), 136(s), 160(sh), 237(w), 302(m,b), 493(s), 580(m,b)	Present work
0.45	635	β_1-$Bi_6Pb_2O_{11}$	Major	55(s), 95(w), 138(w), 302(w,b), 433(w), 495(m), 562(m,b)	Present work
0.50	650	β_2-$Bi_8Pb_5O_{17}$	Major	55(s), 82(sh), 115(sh), 146(s), 220(w,b), 331(w,b), 498	Present work
0.555	600	β_2-$Bi_8Pb_5O_{17}$	Major	54(s), 80(sh), 145(s), 219(w,b), 328(w,b), 498(m), 565 (sh)	Present work
0.60	600	β_2-$Bi_8Pb_5O_{17}$	Major	55(s), 84(sh), 143(vs), 222(w), 330(w,b), 495(m), 567(w,b)	Present work
0.65	630	β_2-$Bi_8Pb_5O_{17}$	Major	88(w), 97(w), 141(s), 235(w), 325(w,b), 495(m), 565(sh)	Present work
0.70	630	β_2-$Bi_8Pb_5O_{17}$	Major	142(s), 207(w), 330(w,b), 497(m,b), 565(sh,b)	Present work
0.75	630	β_2-$Bi_8Pb_5O_{17}$	Major	46(w), 249(w,b), 330(w,b), 500(w,b), 560(sh)	Present work
		PbO	Major	60(sh), 74(w), 87(m), 144(vs), 290(w), 430(vw)	Present work
0.8	630	PbO	Major	69(w), 84(m), 142(s), 284(m), 373(w), 421(vw)	Present work
		β_2-$Bi_8Pb_5O_{17}$	Minor	224(w), 331(vw), 500(w), 560(w,b), 592(sh)	Present work
1	Lab reagent	PbO		55(w), 71(w), 88(s), 101 (vw), 144(vs), 170(sh), 203(vw), 251(sh), 290(s), 386(w), 425(w)	Present work
1	Single crystal	PbO		52(w), 72(s), 87(s), 144(vvs), 171(sh), 217(vw), 250(vvw), 298(vvs), 385(m), 424(w)	[24]

w = weak, vw = very weak, vvw = very very weak, m = medium, s = strong, vs = very strong, vvs = very very strong, b = broad, sh = shoulder.

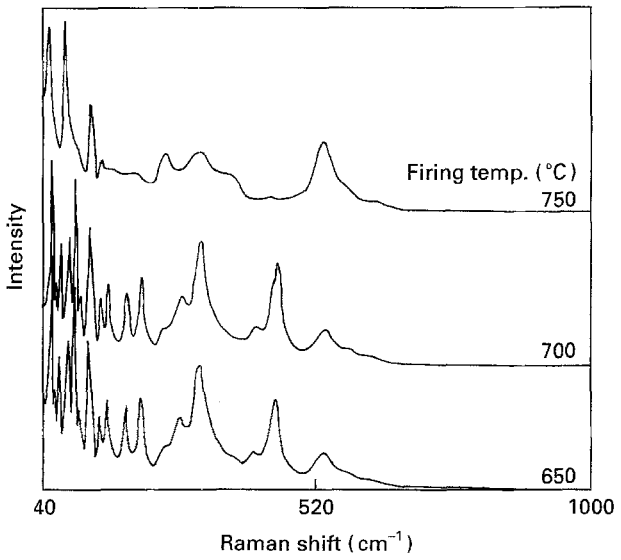

Figure 2 Raman spectra of $(Bi_2O_3)_{1-x}(PbO)_x$, where $x = 0.143$ fired at different temperatures.

65 (sh), 80 (vs), 94 (sh) 125 (s), 144 (m), 171 (w), 204 (w), 258 (w), 315 (m), 355 (w), 378 (w), 450 (vw), 499 (sh), 530 (sh), 562 (sh), 592 (w), 620 (w) and 825 (vw), where sh = shoulder, vs = very strong, s = strong, m = medium, w = weak and vw = very weak. Bands below $\sim 200\,cm^{-1}$ are very sharp, whereas those above are typically much broader for the spectrum at 21 °C. These higher wavenumber bands can be seen to comprise many overlapping bands, resolved at low temperature. This composition has previously been assigned [15] to the sillenite phase, γ-$Bi_{12}PbO_{19}$; however, because of the number of bands observed and the wide compositional stability range, this seems unlikely. The composition is more likely to be that of a solid solution, as discussed earlier.

Low-temperature Raman spectra of $x = 0.4$ (Fig. 4b) reveals a third band in the grouping between $\sim 130 - 160\,cm^{-1}$, at $144\,cm^{-1}$. The band at $298\,cm^{-1}$ is resolved to show at least four components at 237 (sh), 260 (sh), 299 (sh) and 370 (sh). Also, the broad asymmetric profile on the high wave number side of the band at $491\,cm^{-1}$, consists of several components. The other feature of the low-temperature Raman spectra is the increase in the relative intensity of the higher wave number bands. This phenomenon has been observed for α-Bi_2O_3 and the large band widths at room temperature have been attributed to structural disorder [15], giving rise to mixing of phonon states, similar to that which occurs in glasses or crystals with a high defect concentration [20, 21].

When $x = 0.555$ (Fig. 4c), the low-temperature Raman spectra reveal the bands at 87 and $254\,cm^{-1}$ more clearly and shoulders at ~ 120 and $363\,cm^{-1}$, are observed. No evidence of PbO or α-Bi_2O_3 is detected at this temperature, as shown in Fig. 4c.

The low-temperature Raman spectra for $x = 0.75$ is given in Fig. 4d. This shows more clearly that the system is not a single phase, as reported by Biefeld and White [10], but a mixture of PbO which has distinctive bands at 142, 291 and $430\,cm^{-1}$, and β_2-$Bi_8Pb_5O_{17}$ with distinctive bands at ~ 44 and

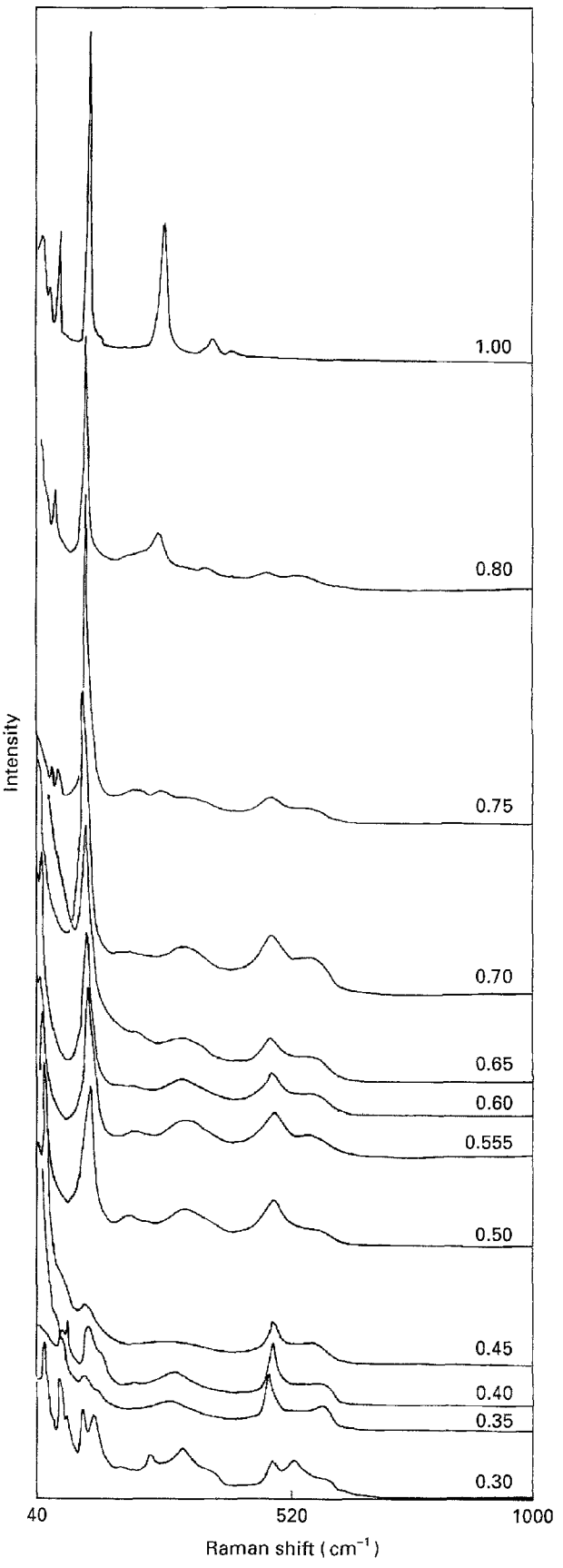

Figure 3 Raman spectra of $(Bi_2O_3)_{1-x}(PbO)_x$, where $x = 0.30$–1.00.

$500\,cm^{-1}$. However, there appears to be another as-yet unidentified component, represented by a band at $255\,cm^{-1}$.

Fig. 5 shows the infrared (i.r.) spectra for the composition range $x = 0.05$–0.25 which are compared with the absorbance profile of monoclinic α-Bi_2O_3.

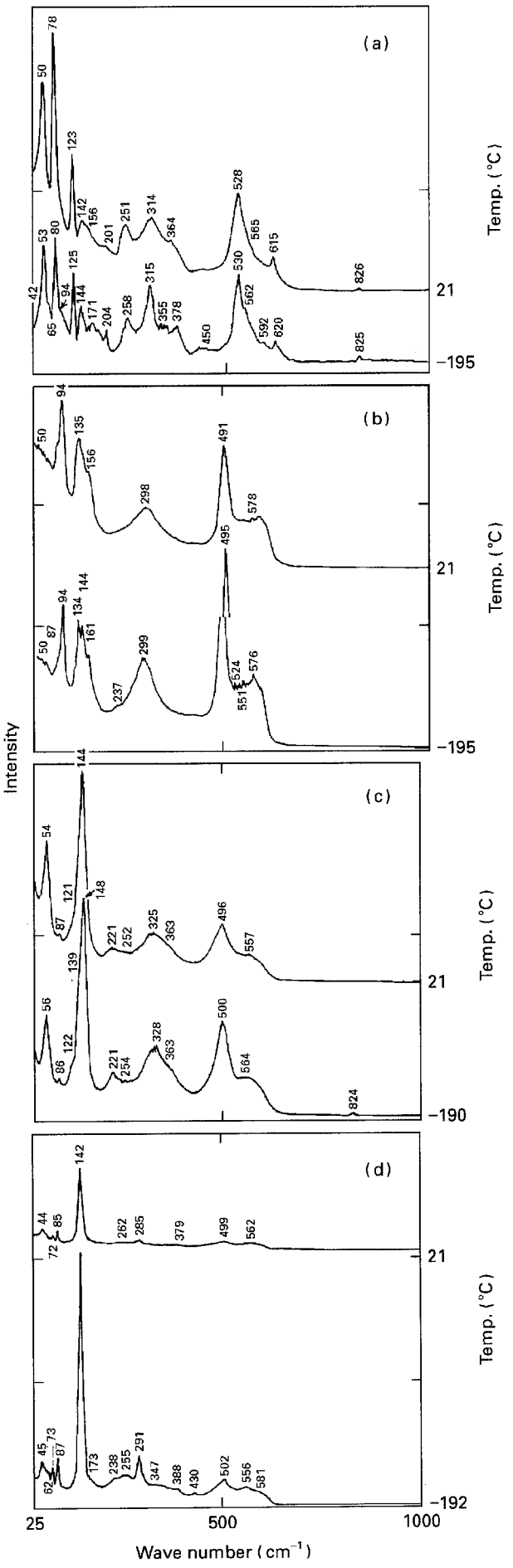

Figure 4 Comparison of Raman spectra at room temperature (21 °C) and low temperature (− 195 °C) of $(Bi_2O_3)_{1-x}(PbO)_x$, where (a) $x = 0143$, (b) $x = 0.40$, (c) $x = 0.555$ and (d) $x = 0.75$.

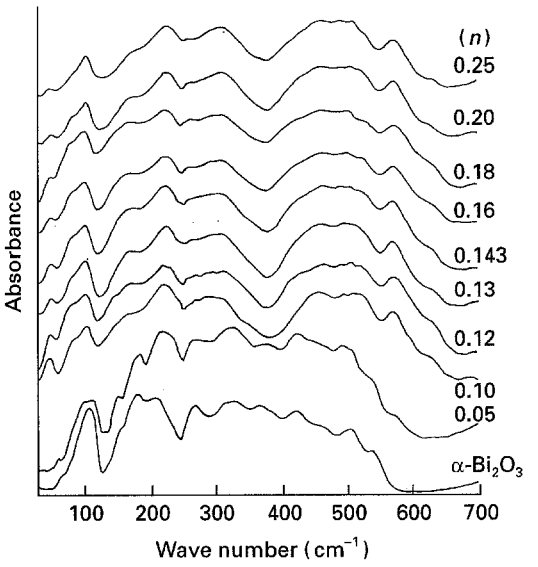

Figure 5 Infrared spectra of $(Bi_2O_3)_{1-x}(PbO)_x$, where $x = 0.00$–0.25 (α-Bi_2O_3).

Table II also lists the i.r. band positions, as well as the quenching temperature, for all the samples examined. This system shows a complex spectrum of 12 bands. At $x = 0.05$, the spectrum shows the presence of α-Bi_2O_3. However, owing to the broadening of the bands at higher PbO concentrations, it can be assumed that the presence of α-Bi_2O_3 is less distinct. The broadness and band contours can be postulated as being due to the particle size and Fröhlich surface mode effects that typically modify i.r. spectra of polar compounds [15]. Nevertheless, at a composition between $x = 0.1$ and 0.2, the i.r. profile is consistent with that assigned to γ-$Bi_{12}PbO_{19}$ [15]. Hence, the composition appears to consist mainly of this phase over the composition range. As with the Raman spectra, this is indicative of a solid solution rather than a single compositional phase. A weak band at 268 cm^{-1} indicates that small amounts of α-Bi_2O_3 were present.

Fig. 6 shows the infrared spectra for the composition range $x = 0.3$–1.0, and Table II lists the band positions. The i.r. spectra for $x = 0.25$ indicate that a slight profile change is present, namely a decrease in the intensity of the band at $\sim$87 cm^{-1}. As with the Raman profiles, there is a distinctive change between $x = 0.25$ and 0.3. With increasing PbO content, in the material, the bands at 120, 210, 296, 424 and 595 cm^{-1} maximize at $x = 0.555$, attributable to the β_2-phase, while at $x = 0.4$ there were eight bands (between $\sim$50 and 650 cm^{-1} absorption envelope) that were attributed to the β_1-phase.

At high PbO content ($x > 0.65$), the profile changes to give broad bands at $\sim$110, 201, 310, 431 and 450 cm^{-1}. These spectra can be compared to those of the PbO system which typically has broad-band spectrum with strong bands observed at 163, 286 and 349 cm^{-1}. Apart from these, several other features exist in the high PbO samples that indicate the presence of PbO, namely bands at 310, 355 and 505 cm^{-1}; hence compositions between $x = 0.65$ and 0.8 appear to contain mainly PbO and the β_2-phase.

TABLE II Infrared band positions of Bi_2O_3 and Bi_2O_3–PbO at room temperature

PbO:Bi_2O_3 (n)	Preparation description	Compound	Phase	Infrared band positions (relative intensity) [mode] (cm^{-1})	Reference
0	Lab reagent	α-Bi_2O_3	Major	68 (sh), 108(s), 155(sh), 209(s), 270(m), 328(m), 367(m), 380(sh), 422(m), 446(sh), 505(m), 535(sh),	Present work
0	Lab reagent	α-Bi_2O_3	Major	39, 58, 62, 67, 100, 116, 132, 186, 214, 283, 380, 425, 465, 510, 540, 595	[15]
0.143	700 °C for 24 h	$Bi_{12}PbO_{19}$		47, 82, 106, 110, 170, 222, 300, 465, 520, 575, 630	[15]
0.05	750 °C for 2 h and quenched	α-Bi_2O_3	Major	61(w), 111(s), 151(w), 182(m), 218(s), 270(w), 327(s), 376(m), 426(m), 507(sh), 534(sh)	Present work
					Present work
		$Bi_{12}PbO_{19}$	Minor	85(sh), 101(sh), 446(sh), 495(m), 567(sh)	Present work
0.10	750	$Bi_{12}PbO_{19}$	Major	45(w), 85(sh), 104(m), 171(sh,b), 224(s), 238(sh), 292(m,b), 340(sh), 457(s), 500(s), 515(s), 570(m), 627(sh)	Present work
0.12	750	$Bi_{12}PbO_{19}$	Major	50(w), 82(sh), 101(m), 169(m), 223(s), 240(sh), 295(s,b), 418(sh), 462 (s,b), 506(s,b), 573(m), 627(sh)	Present work
0.13	750	$Bi_{12}PbO_{19}$	Major	50(w), 85(sh), 102(m), 171(m), 226(s), 310(m), 462(m,b), 502(m,b), 573(m), 618(sh)	Present work
		α-Bi_2O_3	Minor	274(sh)	Present work
0.143	650	$Bi_{12}PbO_{19}$	Major	50(w), 85(sh), 103(m), 175(m), 224(s), 302(m), 343(sh), 434(sh), 468(m,b), 502(m, b), 572(m), 623(sh)	Present work
		α-Bi_2O_3	Minor	247(sh)	Present work
0.143	700	$Bi_{12}PbO_{19}$	Major	51(w), 85(sh), 101(m), 176(m), 225(s), 309(s,b), 465(s,b), 502(s,b), 525(sh), 574(m), 619(sh)	Present work
		α-Bi_2O_3	Minor	268(sh))	Present work
0.143	750	$Bi_{12}PbO_{19}$	Major	48(w), 86(sh), 102(m), 177(m), 223(s), 268(w), 309(s,b), 340(sh), 434(sh), 466(s,b), 510(s,b), 530(sh), 574(m), 623(sh)	Present work
0.16	750	$Bi_{12}PbO_{19}$	Major	51(w), 82(sh), 102(m), 168(sh), 225(s), 311(s,b), 463(s,b), 491(s), 508(s), 573(m), 614(sh)	Present work
		α-Bi_2O_3	Minor	269(w)	Present work
0.18	750	$Bi_{12}PbO_{19}$	Major	49(w), 85(sh), 104(m), 168(sh), 225(s), 259(w), 310 (s,b), 466(s,b), 491(s), 510(s), 573(m), 621(sh)	Present work
0.20	750	$Bi_{12}PbO_{19}$	Major	49(w), 86(sh), 102(m), 177(sh), 225(s), 268(sh), 301 (sh), 311(s), 463(sh), 491(s), 506(s), 520(sh), 572(s), 624(sh)	Present work
		β_2-$Bi_8Pb_5O_{17}$	Minor	433(sh)	Present work
0.25	700	$Bi_{12}PbO_{19}$	Major	47(w), 87 (sh), 104(m), 167(sh), 227(s), 310(s), 465(s), 491(s), 511(s), 574(m), 622(sh)	Present work
		β_2-$Bi_8Pb_5O_{17}$	Minor	71(sh), 258(w)	Present work
0.30	700	$Bi_{12}PbO_{19}$	Major	93(m), 220(s), 266(w), 292(s,b), 308(s), 415(sh)	Present work
		β_2-$Bi_8Pb_5O_{17}$	Major	30(sh), 135(sh), 243(s), 469(s), 521(sh)	Present work
0.35	690	β_1-$Bi_6Pb_2O_{11}$	Major	40(w), 65(w), 93(sh), 127(m), 214(sh), 255(s), 309(sh), 242(sh), 467 (s), 523(sh), 534(s)	Present work
0.40	670	β_1-$Bi_6Pb_2O_{11}$	Major	70(sh), 97(m), 237(s), 290(s,b), 413(m), 468(s), 510(w), 539(m)	Present work
0.45	635	β_1-$Bi_6Pb_2O_{11}$	Major	34(w), 96(m), 134(sh), 174(sh), 237(s), 304(sh), 358(sh), 432(sh), 465(sh), 465(s), 509(w), 532(m)	Present work
0.50	650	β_2-$Bi_8Pb_5O_{17}$	Major	48(sh), 72(sh), 96(sh), 120(s), 203(s), 275(sh), 294(s), 310(sh), 362(w), 424(s), 462(s), 503(sh), 531(w), 595(m)	Present work
0.555	600	β_2-$Bi_8Pb_5O_{17}$	Major	40(sh), 73(sh), 93(sh), 120(s), 179(sh), 210(s), 273(sh), 296 (s), 374(sh), 427(s), 458(s), 519(sh), 591(m)	Present work
0.60	600	β_2-$Bi_8Pb_5O_{17}$	Major	40(w), 73(sh), 113(s), 202(s), 274(sh), 300(s,b), 427(sh), 446(sh), 498(sh), 533(sh), 593(m)	Present work
0.65	630	β_2-$Bi_8Pb_5O_{17}$	Major	39(w), 88(sh), 117(s), 178(sh), 206(s), 273(sh), 363(sh), 418(s), 460(sh), 525(sh), 580(sh)	Present work
		PbO	Minor	310(s), 505(sh)	Present work
0.70	630	β_2-$Bi_8Pb_5O_{17}$	Major	41(w), 73(sh), 115(s), 208(s), 430(s), 470(sh), 565(w)	
		PbO	Minor	302(s,b), 355(s), 505(s)	Present work
0.75	630	β_2-$Bi_8Pb_5O_{17}$	Major	110(s), 201(s,b), 236(sh), 310(m,b), 431(s), 450(s), 567(sh)	Present work
		PbO	Major	505(sh)	Present work
0.80	630	PbO	Major	70(sh), 230(sh), 272(sh), 292(m), 339(m,b), 505(sh)	Present work
		β_2-$Bi_8Pb_5O_{17}$	Minor	113(m), 209(s), 410(m,b), 478(sh), 522(sh), 580(sh)	Present work
1	Lab reagent	PbO		64(sh), 93(sh), 116(w), 163 (s), 219(w), 240(w), 270(sh), 286(s), 349(m), 384(sh), 459(sh), 504(sh)	Present work
1	Powder mull	PbO		290, 356, 500	[24]
1	Single crystal	PbO		146 [TO], 170 [LO], 177 [TO], 279 [TO], 320 [LO], 347 [TO], 486 [LO]	[24]

w = weak, m = medium, s = strong, b = broad, sh = shoulder.

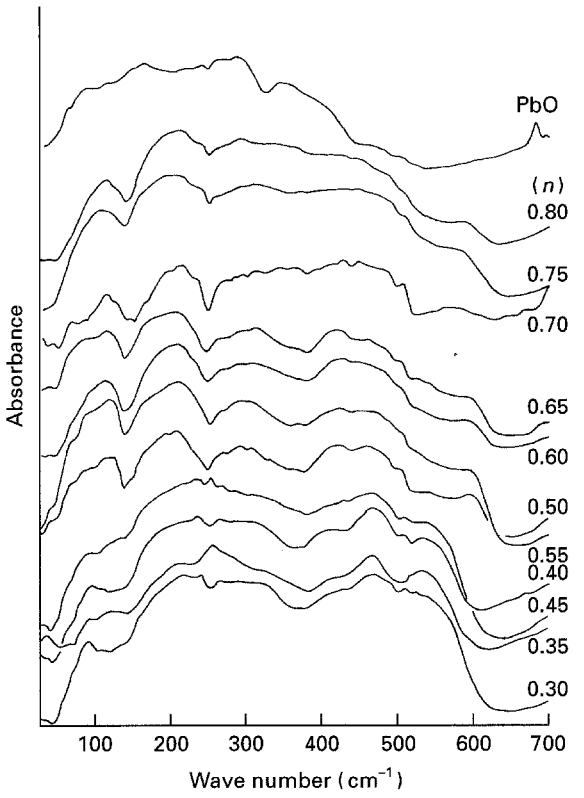

Figure 6 Infrared spectra of $(Bi_2O_3)_{1-x}(PbO)_x$, where $x = 0.30$ –1.00 (γ-PbO).

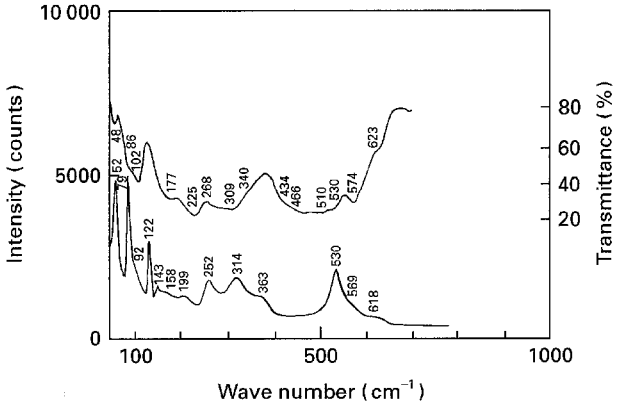

Figure 7 Comparison of infrared and Raman spectra of $(Bi_2O_3)_{1-x}(PbO)_x$, where $x = 0.143$, the δ-solid solution composition.

Fig. 7 shows the i.r. and Raman spectra at $x = 0.143$, in which the composition $Bi_{12}PbO_{19}$ has been reported to exist [10]. This has been observed in this work to be a solid solution, able to be stabilized by quenching from the δ-Bi_2O_3 and δ-Bi_2O_3 + β regions. The Raman spectra show a total of 13 bands. The i.r. spectrum also shows a total of 14 features. The bands at 314, 530, 569 and 618 cm^{-1} appear to be coincident in both the i.r. and Raman. This comparison has been reported by Betsch and White [15] who noted a very short apical Bi–O bond corresponding to the low wavenumber band observed in the spectrum. It was also assumed that no longitudinal–transverse optical splitting occurred at room temperature, because the separation was predicted at 2–10 cm^{-1} [22].

At $x = 0.40$, in Fig. 8, eight i.r. and nine Raman bands are observed with coincident bands at ~96, 237, 302 and 500 cm^{-1}. Because there are only a few bands and high coincidence, the compound has been assumed to be single phase, with considerable symmetry. The bands at 302 and 580 cm^{-1}, in the Raman spectrum, are very broad and have been shown to comprise many components at low temperature,

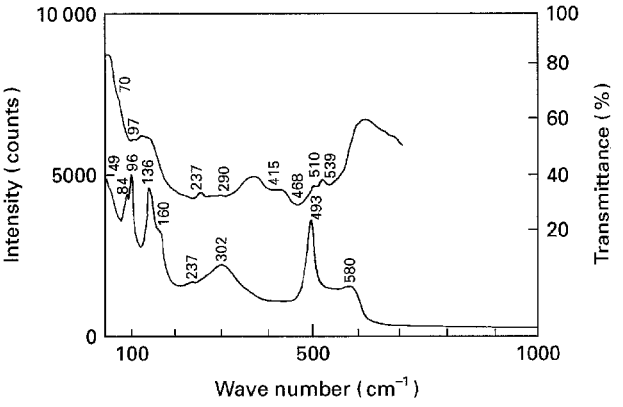

Figure 8 Comparison of infrared and Raman spectra of $(Bi_2O_3)_{1-x}(PbO)_x$, where $x = 0.40$, the β_1-solid solution composition.

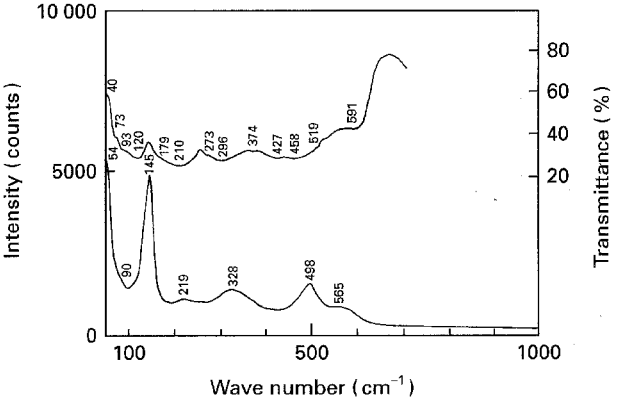

Figure 9 Comparison of infrared and Raman spectra of $(Bi_2O_3)_{1-x}(PbO)_x$, where $x = 0.555$, the β_2-solid solution composition.

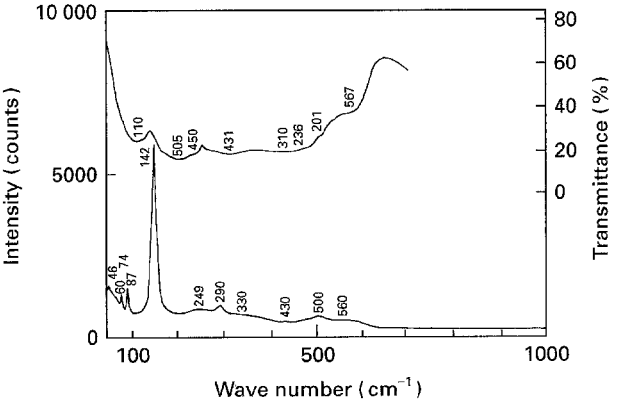

Figure 10 Comparison of infrared and Raman spectra of $(Bi_2O_3)_{1-x}(PbO)_x$, where $x = 0.75$.

where 14 features are discernible. The broad bands are typically attributed to structural disorder in the solid due to the random substitution of cations. This disorder has been described by Betsch and White [15] as arising from the orientation of the space filling by the non-bonding lone-pair orbital of the Bi^{3+} or Pb^{2+} ion.

Fig. 9 shows that at $x = 0.555$, seven Raman and 13 i.r. bands are observed with little evidence of coincident bands present, except at 219 and 498 cm^{-1} coincident with 210 and 519 cm^{-1}, in the infrared spectrum. The system $\beta_2Bi_8Pb_5O_{17}$ has been reported as having a tetragonal structure with cell parameters $a = 0.4041$ and $c = 0.5023$ nm [12]. If the Raman profile is compared to that of tetragonal titanium dioxide [23] (anatase, TiO_2) a similar profile is observed. One of the intense low wavenumber bands at 148 cm^{-1} occurs in both the 144 cm^{-1} band of TiO_2 and similar weak high wave number bands between 300 and 600 cm^{-1}.

Fig. 10 shows the comparison of i.r. and Raman for the system at $x = 0.75$. The evidence here suggests that the structure contains a mixture of mainly PbO and β_2-$Bi_8Pb_5O_{17}$. A total of 11 bands are observed in the Raman profile compared to eight features in the absorption envelope in the infrared spectrum. The bands in the infrared spectrum are very broad and hence it is very difficult to distinguish distinct features, unlike that of the Raman spectrum. However, bands at 60, 74, 87, 144, 290 and 430 cm^{-1} have been attributed to PbO from the infrared spectrum.

Fig. 11 summarizes the results given by the i.r. and Raman spectra, in the form of a phase diagram. The quench lines show the phase at which the sample was heated to and quenched from. The room-temperature phases are given as phase-stability ranges.

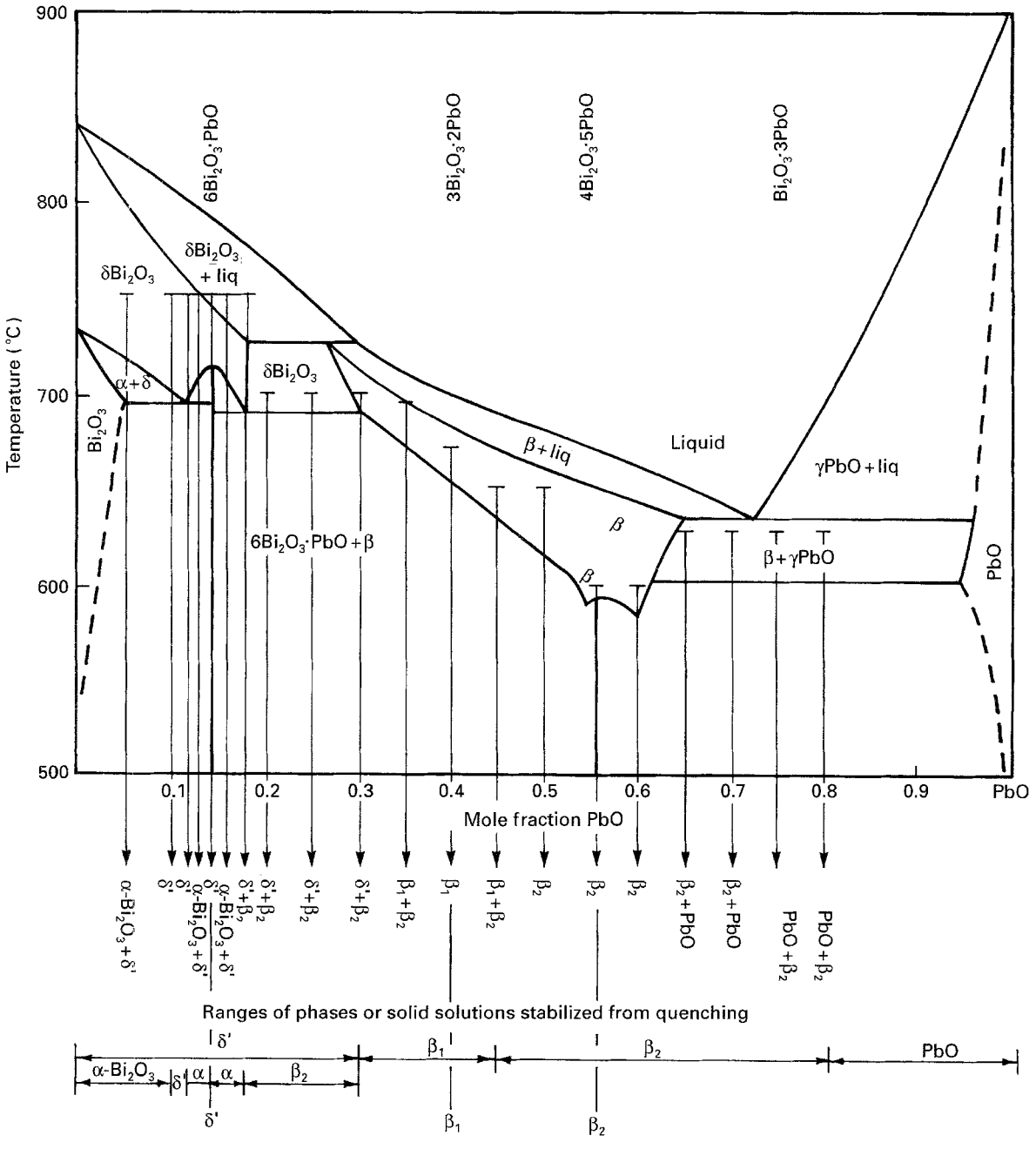

Figure 11 Temperature/composition phase diagram of the system $(Bi_2O_3)_{1-x}(PbO)_x$, with specific quench lines and stabilized room-temperature phase ranges.

4. Conclusion

Detailed Raman and infrared spectra have been obtained for the system $(Bi_2O_3)_{1-x}(PbO)_x$ from $x = 0-1$, at room temperature, after having been quenched from the high-temperature phase. The spectra are reasonably consistent with the previously published phase diagrams; however, as shown in the proposed room-temperature phase diagram, there are some discrepancies. This is particularly apparent for the γ-$Bi_{12}PbO_{19}$ solid solution which was previously proposed as being a single phase. Further studies are currently underway to investigate the high-temperature vibrational spectroscopy and how this oxide system is affected by the application of an overpotential.

References

1. J. A. KILNER, J. DRENNAN, P. DENNIS and B. C. H. STEELE, *Solid State Ion.* **5** (1981) 527.
2. H. A. HARWIG and A. G. GERARDS, *J. Solid State Chem.* **26** (1978) 265.
3. H. KRUIDHOF, K. SESHAN, B. C. LIPPENS Jr, P. J. GELLINGS and A. J. BURGGRAAF, *Mater. Res. Bull.* **22** (1987) 1635.
4. T. TAKAHASHI, H. IWAHARA and T. ARAO, *J. Appl. Electrochem. Soc.* **5** (1975) 187.
5. N. M. SAMMES and G. J. GAINSFORD, *Solid State Ion.* **62** (1993) 179.
6. P. SU and A. VIRKAR, *J. Electrochem. Soc.* **139** (1992) 1672.
7. T. TAKAHASHI, H. IWAHARA and Y. NAGAI, *J. Appl. Electrochem. Soc.* **2** (1972) 97.
8. E. M. LEVIN and R. S. ROTH, *J. Res. Nat. Bur. Stand. A. Phys. Chem.* **68A** (1964) 197.
9. J. BOIVIN and G. TRIDOT, *Compt. Rend.* **278** *ser C* (1974) 865.
10. R. M. BIEFELD and S. S. WHITE, *J. Am. Ceram. Soc.* **64** (1981) 182.
11. N. M. SAMMES, R. J. PHILLIPS and M. G. FEE, *Solid State Ion.* **69** (1994) 121.
12. F. HONNART, J. C. BOIVIN, D. THOMAS and K. J. DeVRIES, *ibid.* **9, 10** (1983) 921.
13. L. G. SILLEN and R. AURIVILLIUS, *Nature* **155** (1945) 305.
14. J. C. BOIVIN, D. THOMAS and G. TRIDOT, *Compt. Rend* **268** *ser C* (1969) 1149.
15. R. J. BETSCH and W. B. WHITE, *Spectrochim. Acta.* **34A** (1978) 505.
16. F. D. HARDCASTLE and I. E. WACHS, *J. Solid State Chem.* **97** (1992) 319.
17. *Idem, J. Phys. Chem.* **95** (1991) 10763.
18. Z. WUZONG, D. A. JEFFERSON, M. ALARIO-FRANCO and J. M. THOMAS, *ibid.* **91** (1987) 512.
19. L. DIXIT, D. L. GERRARD and H. J. BROWLEY, *Appl Spectrosc. Rev.* **22** (1986) 189.
20. S. A. BRAWER and W. B. WHITE, *J. Chem. Phys.* **63** (1975) 2421.
21. V. G. KERAMIDAS and W. B. WHITE, *J. Phys. Chem. Solids* **34** (1973) 1873.
22. S. VENUGOPALAN and A. K. RAMDAS, *Phys. Rev. B* **5** (1972) 4065.
23. T. OHSAKA, F. IZUMI and Y. FUJIKI, *J. Raman Spectrosc.* **7** (1978) 321.
24. D. M. ADAMS and D. C. STEVENS, *J. Chem. Soc. Dalton* (1977) 1096.

Received 23 August 1994
and accepted 22 March 1995